Transfer-length method measurements under variable illumination to investigate hole-selective passivating contacts on c-Si(p) and c-Si(n) wafers

Laurie-Lou Senaud[1,2], Luca Antognini[2], Gabriel Christmann[1], Mathieu Boccard[2], Matthieu Despeisse[1], Christophe Ballif[1,2] and Bertrand Paviet-Salomon[1]

***Abstract*—In this work, TLM measurements under variable illumination are applied to study p-type carrier selective passivating contacts (CSPCs) employed in the silicon heterojunction (SHJ) technology. In the case of p-type CSPCs deposited on p-type crystalline silicon (c-Si(p)) wafers, we demonstrate that illumination has a strong impact on the contact resistivity (ρ_c) value, as demonstrated in our previous contribution in the case of n-type CSPCs on c-Si(n). Noticeably, it was again found that ρ_c increases and that the c-Si sheet resistance (R_{sh}) decreases with the illumination. In addition, we demonstrate that ρ_c is impacted differently by illumination depending on the doping of the p-type thin hydrogenated silicon layer. Then, we investigate and discuss the applicability of TLM measurements under illumination to measure p-type CSPCs deposited on their inverse type c-Si(n) wafers. First, performing TLM measurement in dark condition of such samples allow one to measure R_{sh} values with orders of magnitude corresponding to the c-Si(n) inversion layer one. Second, we demonstrate that under illumination, the lateral transport inside the c-Si(n) bulk is supported by the electrons thanks to two experimental evidences, i.e. that the R_{sh} behavior as function of injection behaves as the one of electrons, and that an electron transport inside the c-Si(n) wafer in the presence of two p-type CSPCs TLM pads can only be mediated thanks to photogeneration under one pad and recombination under the other. These results provide additional understandings of the TLM measurement under illumination as well as strong insights for the investigation of carriers transport and electrical losses in CSPCs solar cells.**

***Index Terms*—Transfer length method, illumination, injection level, carrier selective passivating contacts, carrier transport, inversion layer, recombination mechanisms, silicon heterojunction**

I. Introduction

SILICON heterojunction (SHJ) based solar cells are promising carrier selective passivating contact (CSPC) technologies demonstrating up to 26.7% efficiency in IBC configuration [1]. To reach record efficiency, one important lever is the minimization of the resistive losses. Indeed, when the CSPCs of SHJ solar cells are not properly optimized, important electrical transport losses can occur, strongly capping the solar cell performance [2]. These losses are mainly caused by the electrical transport of carriers and their extraction occurring from the bulk absorber to the terminal electrodes passing through the thin intrinsic and doped hydrogenated silicon, transparent conductive oxide, and metal layers. In particular, these layers induce resistive losses through the bulk of the materials and several energy barriers stemming from discontinuities in the energy band structure, arising at the hetero-interfaces created between the different materials constituting SHJ solar cells [3]. One way to quantify the resistive losses induced by the electrical transport is to measure the contact resistivity value (ρ_c). This parameter characterizes the carrier transport quality through given interfaces and materials composing the solar cells. Any change to the energy barriers or to the bulk properties of the materials constituting the solar cell and of the absorber bulk will directly affect the ρ_c value [3]. The parameter ρ_c reflects then the resistive losses of the carrier transport induced by the global band alignment resulting from the coupling of the different material properties and is therefore a relevant parameter to investigate different interfaces and properties couplings arising between multiple materials [4], [5]. The transfer length method (TLM) is one of the most commonly used techniques to measure the ρ_c of a stack composed of several material layers, such as the CSPCs present in SHJ solar cells [6]–[9]. Currently however, two major gaps of this method have not yet been filled in the literature when studying electrical losses of solar cells. First, the ρ_c characterization is only performed in dark conditions, and secondly, in the case of crystalline silicon (c-Si) based solar cells, it is not possible to measure the ρ_c value of a CSPC presenting the opposite type (n or p-type) to the c-Si bulk of the actual solar cell. Commonly, to measure the ρ_c values of p-type CSPCs, p-type c-Si wafers are used and conversely, to measure the ρ_c values of n-type CSPCs, n-type c-Si wafers are used [10], [11].

The first restriction was studied and elucidated in [4], [12] in the case of n-type CSPCs on n-type c-Si (c-Si(n)), where we demonstrated that the value of ρ_c increases with the illumination, i.e. with the injected carrier density. In the case of p-type CSPCs measured on p-type and n-type c-Si, illumination dependent TLM measurements were reported in [13] and different possible artifacts on the measurement were discussed. However, a description of the physical mechanisms allowing electrical transport in those structures was lacking. The present works addresses this point in more details. Indeed, considering the case of c-Si(n) based solar cells, it is questionable if the

Manuscript received April 19, 2005; revised August 26, 2015.

1 The authors are with the PV-Center, Centre Suisse d'Électronique et de Microtechnique, Neuchâtel CH-2002, Switzerland (e-mail: laurie-lou.senaud@ csem.ch; gabriel.christmann@csem.ch; sylvain.nicolay@csem.ch; matthieu.despeisse@ csem.ch; christophe.ballif@csem.ch; bertrand.paviet-salomon@csem.ch).

2 The authors are with the EPFL STI IMT PVLab, Neuchâtel CH-2002, Switzerland (e-mail: luca.antognini@epfl.ch; mathieu.boccard@epfl.ch).

value of ρ_c of p-type CSPCs measured on p-type c-Si (c-Si(p)) wafers accounts correctly for the actual transport losses once these p-type CSPCs are deposited onto n-type wafers. As a matter of fact, in the particular case of SHJ solar cells the global transport quality is connected to the band bending at the c-Si/a-Si:H(i), a-Si:H(i)/doped hydrogenated silicon layer, and doped hydrogenated silicon layer/TCO interfaces. More specifically, at the vicinity of the c-Si/a-Si:H(i) interface, a change of the c-Si bulk properties, such as a change of its charge-carrier density or charge-carrier type (i.e. a Fermi or quasi-Fermi level change inside the c-Si bulk), will affect the local band bending inside the c-Si bulk and thus affect the accumulation of carriers at the vicinity of the c-Si/a-Si:H(i) interface, potentially impacting the ρ_c value. In other words, for a given CSPC, the value of ρ_c is expected to depend strongly on the charge-carrier density and charge-carrier type inside the c-Si bulk. This forms the rationale of our investigation.

First, the ρ_c behaviour under variable illumination of p-type CSPC deposited on c-Si(p) wafers is studied as it was done in [4] for the case of n-type CSPCs deposited on c-Si(n) wafer. As introduced above, the study of the resistive transport losses induced by p-type CSPCs in SHJ solar cells is commonly carried out using c-Si(p) wafers which play the role of the conductive layers to perform contact resistivity measurements, as it is not possible to perform such measurements directly on c-Si(n) wafers [10], [11]. Indeed, in this case, the p-n junction created between the p-type CSPC and the c-Si(n) wafer makes it impossible to perform contact resistivity measurements in dark conditions, neither using TLM nor symmetric vertical structures [10], [11]. This is why any CSPCs under study are commonly characterized when deposited on a wafer of the same doping type, i.e. here p-type CSPCs would be studied when deposited on c-Si(p). Second, based on the results presented in [4], the applicability of TLM measurements under variable illumination to the case of p-type CSPC deposited on c-Si(n) wafers is investigated. Indeed, as the coupling of p-type CSPC deposited on c-Si(p) wafers is expected to differ from when deposited on c-Si(n) wafers, TLM measurement under variable illumination was applied to samples featuring a p-type CSPC deposited on a c-Si(n) wafer.

For this study, three different p-type thin hydrogenated amorphous silicon (a-Si:H(p)) layers were integrated in CSPCs configuration deposited either on c-Si(p) or on c-Si(n) wafers (hereafter referred as p/P and p/N respectively) as presented in Figure 1a. TLM measurements were performed in the dark and under variable illumination as presented in [4] for a-Si:H(p) layers processed with different TMB flows. The ρ_c values obtained for both p/P and p/N cases in the dark and under variable illumination are studied and compared. Finally, large TLM samples are studied to investigate further the physical mechanisms behind the carrier transport inside the c-Si(n) bulk of the p/N TLM architecture.

II. Experimental details

TLM samples were fabricated on textured c-Si(n) and c-Si(p) wafers presenting resistivities of 3.0 and $11.5\,\Omega\,\mathrm{cm}$ and thicknesses of $170\,\mu\mathrm{m}$ and $160\,\mu\mathrm{m}$, respectively. On the front side of the TLM samples, a thin blanket of intrinsic hydrogenated silicon layer (a-Si:H(i) or i) was deposited and then completed with a thin p-type hydrogenated silicon layer (a-Si:H(p) or p) which was processed with three different TMB flows, namely low (50 sccm), medium (75 sccm) and high (100 sccm) to obtain three different a-Si:H(p) layer dopings while keeping a constant thickness of $12\,\mathrm{nm}$ measured on planar glass substrate. The activation energies (E_a) of the three a-Si:H(p) layers were determined by conducting temperature-dependent dark conductivity measurements [14] and present values of 426, 365 and $341\,\mathrm{meV}$ for the low, medium and high TMB flows, respectively. This parameter E_a is equal to the energy difference between the Fermi level and the current transporting band, i.e., the conduction band for the case of electrons and the valence band for the case of holes. Thus, the lower the E_a, the higher the doping of the thin silicon layer. A thin a-Si:H(i) layer was deposited to passivate the rear-side of the TLM samples, followed by a silicon nitride SiN_xlayer (see Figure 1). The thickness of the SiN_xlayer measured on planar bare glass substrate was about $120\,\mathrm{nm}$ which leads to an optimal thickness for antireflecting coating (ARC) on textured wafer. The combination of a-Si:H(i)/SiN_xstack at the rear side of the TLM samples allows one to reach a good passivation quality together with an optimized ARC, and thus to maximize the injected carrier concentration reached inside the c-Si bulk of the TLM samples for a given illumination. In addition, the presence of the a-Si:H(i)/SiN_xstack, as presented in Figure 1, prevents any TLM current to go through the rear layers, hence restricting it to the c-Si bulk. Following this step, aluminium-doped zinc oxide (AZO) was deposited on the front side of the TLM samples on the different a-Si:H(p) layers. This AZO layer features a thickness of $180\,\mathrm{nm}$ on planar glass substrate and a carrier concentration of $4.42\times10^{19}\,\mathrm{cm}^{-3}$. Finally, a $400\,\mathrm{nm}$-thick silver (Ag) layer was sputtered over the whole front AZO layer. After this step, the TLM samples were annealed at $210\,^{\circ}\mathrm{C}$ for $30\,\mathrm{min}$ to mimic the annealing occurring during the screen-printing process in solar cells fabrication. Then, TLM patterns featuring a length (L) of $2\,\mathrm{mm}$ as well as gaps of 0.25, 0.50, 0.75, 1.00, 1.25, 1.50 and $2.00\,\mathrm{mm}$ were inkjet-printed. The Ag and AZO layers were then etched between the pads, and the ink was removed. After these etching steps, the TLM samples were cut with a selected width (w) of $6\,\mathrm{mm}$ to create the mesa isolation. *I-V* measurements were performed on each completed TLM sample in dark conditions and under different illumination intensities, namely, 7%, 13%, 50%, and 100% of equivalent AM1.5G one sun intensity, to reach different injected carrier densities inside the c-Si bulk. The TLM samples were illuminated at the rear-side using a flip table to ensure a homogeneous injection between and below each TLM pad (see [4]). From the I–V curves, the TLM computation was performed, and the the contact resistivity (ρ_c) as well as the sheet resistance (R_{sh}) were extracted. Finally, corrections on the value of ρ_c considering the wafer thickness of the TLM samples were performed for each TLM measurement, as presented in [15]. Eventually, for each illumination, the injected carrier density values were calculated from the sheet resistance (R_{sh}) of the

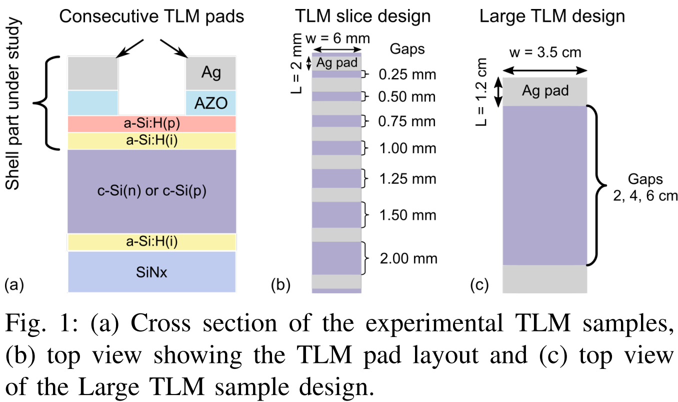

Fig. 1: (a) Cross section of the experimental TLM samples, (b) top view showing the TLM pad layout and (c) top view of the Large TLM sample design.

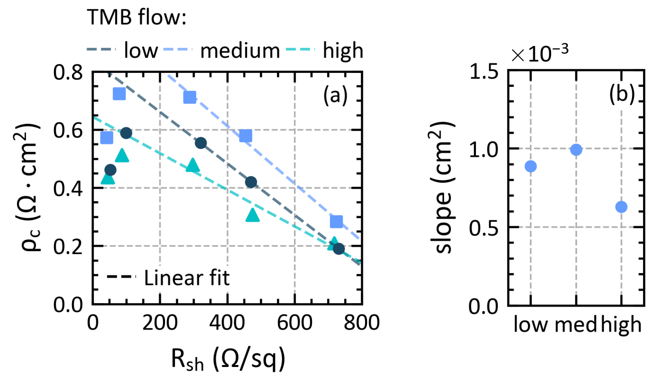

Fig. 2: (a) ρ_c as a function of the illumination-impacted R_{sh} for the three a-Si:H(p) layers with the different TMB flows, namely low, medium and high, respectively, and deposited on c-Si(p) wafer. From right to left, each R_{sh} value is related to one of the five illuminations which are dark, 7%, 13%, 50% and 100%. (b) Slopes of the linear relation $\rho_c = f(R_{\text{sh}})$, taken in the range of the three lowest illuminations from dark to 13% illumination for the three a-Si:H(p) layers under study.

c-Si wafer, taking into account the dependence of the electron mobility on the injection [16], [17]. More details about our process steps and characterization methods are given in [4], [18]–[20].

Finally, additional test samples, hereafter referred to as large TLM samples, were processed to investigate further the carrier transport properties inside the c-Si(n) bulk of the p/N TLM architecture (see Figure 1c). These large TLM samples were processed on textured c-Si(n) wafer with a resistivity of about $2\,\Omega\,\text{cm}$ and a thicknesses of $190\,\mu\text{m}$. In addition, they underwent similar process steps than the previously described TLM samples, except that the AZO and the Ag depositions were performed using shadow masks, instead of using inkjet printing, to define the pads featuring a length of $1.2\,\text{cm}$ and a width of $3.5\,\text{cm}$ as well as three different gaps of 2, 4 or $6\,\text{cm}$. The large size of these TLM samples allow one to maximize the resistive impact of the bulk with respect to the contacts (i.e., TLM pads) and to minimize the impact of the recombination at the unpassivated edges. The injection level as function of illumination in those samples was measured using a WCT-120 photoconductance decay (PCD) tester [21]. Photoluminescence (PL) images were acquired using a $808\,\text{nm}$ laser to illuminate the samples and a CCD camera coupled with a filter that eliminates the signal from the light source [22]. The formulas used to perform TLM computation and to calculate the sheet resistance as a function of the injection levels are recalled in section IV.

III. Results and Discussion

A. p-type CSPC on c-Si(p) wafers

Figure 2a plots the resulting ρ_c behaviour as a function of the illumination-impacted c-Si R_{sh} for the three CSPCs with the different a-Si:H(p) layers, namely low, medium, and high. As for the case of n-type CSPCs deposited on c-Si(n) wafers presented in [4], the ρ_c is found to increase with the R_{sh} decrease and this dependence presents different slopes for the different a-Si:H(p) layers (see Figure 2b). Note that here the slope is considered for the three lowest illumination. In particular, it is observed that the dark ρ_c value of the p-type CSPC featuring the a-Si:H(p) layer with a medium TMB flow is the highest with a value of $0.28\,\Omega\,\text{cm}^2$, whereas the ones with the low and high TMB flow a-Si:H(p) layers present close values of 0.21 and $0.19\,\Omega\,\text{cm}^2$, respectively. The ρ_c values are in close agreement with the literature [5], [11]. In addition, it is observed that under illumination ρ_c increases up to about +0.3 to $+0.44\,\Omega\,\text{cm}^2$ (from dark to 13% illumination), similarly to what was observed in [4], [12]. Thus, the ρ_c behaviour under illumination of p-type CSPCs on c-Si(p) wafer is found to be similar than the one of n-type CSPCs on c-Si(n) wafer. Considering now the slope of the linear dependence of $\rho_c = f(R_{\text{sh}})$ for the three lowest illuminations, it is observed that the three p-type CSPCs present different illumination responses. Again, this pinpoints that depending on the SHJ sub-material properties, here different a-Si:H(p) layer dopings, the resulting coupling arising between all the SHJ components will shape distinctly the final illumination response, as discussed and illustrated with the concept of *shell* in [4]. In particular, despite the close dark ρ_c values of the a-Si:H(p) layers presenting the low and the high TMB flow, their slopes are significantly different with values of 8.87×10^{-4} and $6.18 \times 10^{-4}\,\text{cm}^2$, respectively. This demonstrates again that under variable illumination, different CSPCs may present distinct illumination responses and thus significantly different transport losses once integrated in real solar cells. Finally, it is important to comment that Figure 2a reveals a drop of ρ_c for the two highest illuminations of 50% and 100%, i.e., for the two lowest R_{sh} values. We believe this drop is correlated to the wafer doping [23] and more in-depth work should be carried in the future to cover this topic.

B. p-type CSPC on c-Si(n) wafers

*1) **Observation of the ρ_c under illumination**:* Figure 3a plots the simulated energy-band diagrams in dark conditions for an a-Si:H(p)/a-Si:H(i) layer stack (denoted p/i here) deposited either on a c-Si(p) (dark blue) or on a c-Si(n) (red) wafer. It is clearly observed and highlighted that the resulting properties coupling of the p/i stack with the two distinct c-

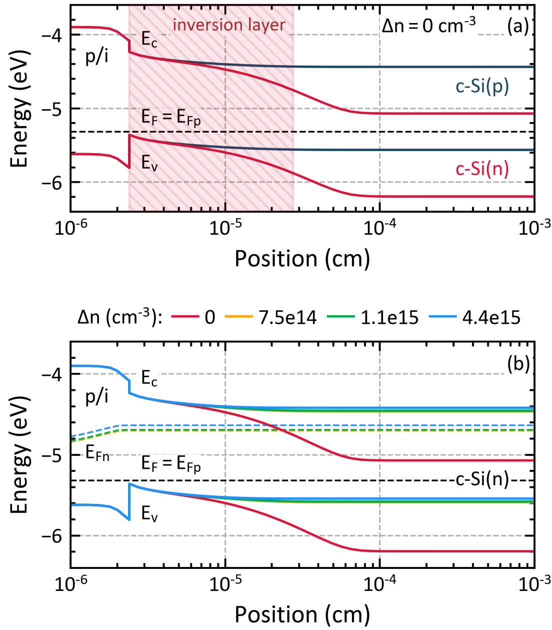

Fig. 3: Simulated energy-band diagrams in the space domain for an a-Si:H(p)/a-Si:H(i) layer stack (denoted p/i here) deposited on (a) a c-Si(p) as well as on a c-Si(n) wafers in dark conditions ($\Delta n = 0\,\mathrm{cm}^{-3}$). (b) p/i layer stack deposited on a c-Si(n) wafers in dark conditions and under three different injection levels of $\Delta n = 7.5{\times}10^{14}$, $1.1{\times}10^{15}$ and $4.4{\times}10^{15}\,\mathrm{cm}^{-3}$. The conduction and the valence band energies (E_c and E_v respectively), as well as the Fermi level (E_F) and both electron and hole quasi-Fermi levels (E_{Fn} and E_{Fp} respectively) are represented spatially. In addition, the inversion layer present inside the c-Si(n) bulk in dark conditions is highlighted in light red dashed area. These energy-band diagrams were simulated with the PC1D software [26].

Si bulks leads to different energy-band alignments and thus, expectedly, to different ρ_c values as introduced in the previous sections. Moreover, in the case of the c-Si(n) wafer, an inversion layer, i.e., a p-type area inside the c-Si(n) bulk [24], [25], here of $252\,\mathrm{nm}$ width, is present and highlighted in light red-dashed area in Figure 3a. Thus, the junction created between the p-type CSPCs (here represented by the p/i layer stack) and the n-type c-Si bulk is clearly visible. Figure 3b plots the energy-band diagrams for the same p/i stack deposited on a c-Si(n) bulk under four different injection levels, from dark with zero injection up to $4.4 \times 10^{15}\,\mathrm{cm}^{-3}$. It is observed that the injected carriers open the blocking junction, i.e., the photogeneration provides free holes, making the n-type c-Si wafer hole-conductive in addition to electron-conductive, and the inversion layer therefore disappears. These injection conditions are thus expected to enable an external applied current, such as the one applied in TLM measurements, to flow in both directions, from the p/i layers to the c-Si(n) bulk and conversely, while additionally flowing through the c-Si(n) bulk thanks to the free generated carriers.

To complete these simulations, Figure 4 shows the experimental *I*-*V* curves obtained between two TLM pads with an

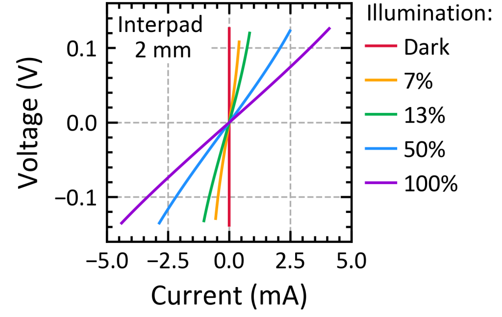

Fig. 4: Experimental *I*-*V* curves for the different illuminations in the case of a TLM gap of $2\,\mathrm{mm}$ and for the high TMB flow a-Si:H(p) layer deposited on c-Si(n) wafer.

TABLE I: Resistance extracted from each *I*-*V* curves presented in Figure 4 for the different illuminations under studies.

Illumination (Suns)	**Resistance (Ω)**
dark	1.01×10^5
7%	2.29×10^2
13%	1.28×10^2
50%	4.69×10^1
100%	3.01×10^1

interpad distance of $2\,\mathrm{mm}$ and for the a-Si:H(p) layer with the high TMB flow. Interestingly, it is observed that the higher the illumination, i.e., the higher the injection level, the higher the resulting current for a same applied voltage, evidencing a decrease of the total resistance with the illumination increase. The variations among the illumination of the total resistance extracted from these *I*-*V* curves are presented in Table I. The total resistance decreases with the illumination increase actually stands from 1.01×10^5 down to $3.01 \times 10^1\,\Omega$. This demonstrates that owing to the injected carriers, the blocking junction is suppressed (as observed by simulation, see Figure 3b), and in addition the c-Si(n) wafer conductivity increases at the same time, thus in overall leading to a decrease of the global resistance encountered by the external TLM current flow.

Following these results, TLM measurements of p-type CSPCs coupled with their inverse n-type c-Si bulk were carried out under variable illumination, for two different a-Si:H(p) layers under study. Figure 5 shows the ρ_c behaviour as a function of the illumination-impacted R_{sh} for the a-Si:H(p) layers featuring a medium or high TMB flow, and deposited on c-Si(n) wafers. Interestingly, here ρ_c is found to decrease with the R_{sh} decrease which is the opposite trend to the one observed with n- or p-type CSPC deposited on c-Si(n) and c-Si(p) wafers, respectively. The ρ_c decreases down to 0.37 and $0.47\,\Omega\,\mathrm{cm}^2$ at 100% illumination for the high and medium TMB flow a-Si:H(p) layers, respectively. In particular, at low illumination, the ρ_c values are found to be very high (up to $6.48\,\Omega\,\mathrm{cm}^2$). These high values result mainly from the impact of the p-n junction present between the p-type CSPC and the c-Si(n) wafer and are not only caused by the heterointerfaces present in the energy-band diagram.

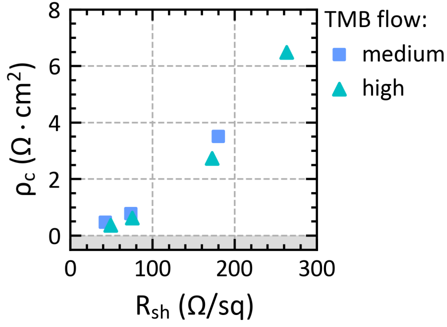

Fig. 5: ρ_c as a function of the illumination-impacted R_{sh} for the CSPCs featuring two different a-Si:H(p) layers, namely with a medium and a high TMB flow, respectively, deposited on c-Si(n) wafer. For a fixed p-type CSPC, each R_{sh} value is related to one of the four illuminations which are 7%, 13%, 50% and 100%, from right to left.

TABLE II: Dark R_{sh} obtained by applying TLM measurement in the dark for the p-type CSPCs featuring two different a-Si:H(p) layers, namely with a medium and a high TMB flow, respectively, deposited on c-Si(n) wafer.

a-Si:H(p) layer	medium	high
R_{sh} dark (Ω/sq)	3.57×10^5	2.82×10^5

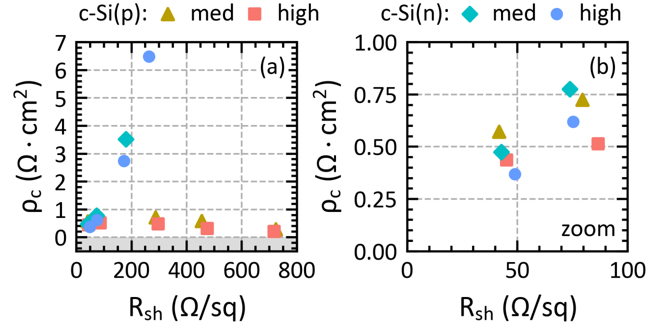

Fig. 6: ρ_c as a function of the illumination-impacted R_{sh} for the two CSPCs with the a-Si:H(p) layers featuring different TMB flows, namely medium (med) and high, respectively, and deposited either on c-Si(n) or c-Si(p) bulk.

TABLE III: ρ_c values for the CSPCs featuring the a-Si:H(p) layers with the two TMB flows, namely medium and high, respectively, and deposited either on c-Si(p) or c-Si(n) wafer in dark conditions and at 50% illumination.

	ρ_c (Ωcm^2)	
a-Si:H(p) doping	medium	high
dark, c-Si(p)	0.28	0.21
50% illum., c-Si(p)	0.72	0.51
50% illum., c-Si(n)	0.77	0.62

Interestingly, in dark conditions, looking at the slope of the total resistance obtained between two TLM pads as a function of the interpad distance, it is observed that this slope presents very high values (data not shown). From this slope, the R_{sh} values can be extracted with high accuracy even if the full TLM computation to extract ρ_c is limited as the total resistance is dominated by the conductive layer own resistance [6]–[9], [27]. Here, the measured R_{sh} presents values of 2.82×10^5 and 3.57×10^5 Ω/sq (see Table II) which is compatible with values reported for the inversion layers of p/N configuration [24] present inside the c-Si(n) bulk in dark conditions (see Figure 3a). Note that the lateral transport inside the a-Si:H(p) layer is prohibited as it features a R_{sh} of about 4.39×10^{10} Ω/sq. This indicates that TLM measurements of p-type CSPCs deposited on their inverse type c-Si(n) bulks allow one to characterize the R_{sh} of the c-Si inversion layer (as must also be the case for n-type CSPC on c-Si(p) bulk). This result may complete other studies for the investigation of the inversion layer properties, as those presented by [24], [25], [28].

Figures 6a and b show the ρ_c values as a function of the illumination-impacted R_{sh} for two p-type CSPCs (high and medium TMB flows) deposited either on c-Si(p) or on c-Si(n) bulks. It results from this comparison that the ρ_c values and trends are different between the c-Si(n) and c-Si(p) cases. This first observation demonstrates that the properties coupling of a p-type CSPC with a given type of c-Si bulk has a non-negligible impact on the resulting value of ρ_c, highlighting the importance of measuring given CSPCs with their appropriate c-Si bulks, i.e. the one used in actual solar cells, in order to accurately consider the physical behaviours and their impact on the resistive transport losses [4]. Note that at sufficiently high illumination, i.e. for low R_{sh} values obtained at 50% and 100% illumination here, the ρ_c values obtained for a given p-type CSPC on c-Si(n) and c-Si(p) wafers are close to each other (see Figure 6b). This could be explained by the fact that both energy-band diagrams (i.e., the p/i/c-Si(n) and p/i/c-Si(p) cases) are similar under illumination. Moreover, at illumination of 50% corresponding to injection close to MPP[1] the ρ_c values obtained for both the c-Si(n) and c-Si(p) cases are higher than the ρ_c values obtained in the case of c-Si(p) in dark conditions (see Table III).

*2) **Observation of the R_{sh} under illumination**:* As a first conclusion, the fact that the ρ_c values obtained on c-Si(n) bulks under illumination are of the same order of magnitude than the ones obtained on c-Si(p) for the two high illuminations of 50% and 100% may strengthen the confidence in the applicability of this new characterisation method to measure accurately the ρ_c value of p-type CSPCs on their opposite c-Si(n) wafer type. However, to further investigate this method, it is important to consider the values of the R_{sh}. Indeed, when looking more closely at the illumination-impacted R_{sh} values for the case of c-Si(n) wafers, it is observed that they are significantly lower than expected when assuming only holes flowing inside the c-Si(n) wafer. Table IV presents the obtained R_{sh} values for the p-type CSPC with the high TMB flow a-Si:H(p) layer along with the calculated injection level considering either the R_{sh} as the one of holes (Δp) or the one of electrons (Δn). It

[1]The 50% illumination in the case of n/N TLM samples with similar c-Si(n) bulk and passivation quality was the illumination giving an injection level of about 2.0×10^{15} cm^{-3}, i.e. close to the maximum power point (MPP) of a given solar cell presented in [4].

is observed that if the obtained R_{sh} is effectively the one of the holes as assumed above, the injection levels are found to be significantly higher for each illumination compared to the ones obtained in the first case study presented in [4] for similar n-type c-Si wafers and passivation quality. These values are recalled in Table V which presents the injected carrier densities obtained in the study [4] and which were expected for the present case study (see column "expected Δn"). Table V gives also the corresponding hole and electron R_{sh} ($R_{\text{sh,h}^+}$ and $R_{\text{sh,e}^-}$ respectively) obtained with these given injection levels. It is observed that the resulting $R_{\text{sh,h}^+}$ values are significantly higher than the ones obtained here experimentally for similar illuminations. Rather, the obtained R_{sh} values presented in Table V are found to closely match the values of $R_{\text{sh,e}^-}$ presented in Table IV for 13%, 50% and 100% illumination. In addition, the injected carrier density calculated considering the obtained R_{sh} as the one of electrons are close to the one obtained in the first case study of [4] for the 13%, 50% and 100% illumination. Note that here, for the case of 7% illumination, the calculation of Δn is not possible as the obtained R_{sh} value is found to be too high to consider electrons flowing through the c-Si(n) wafer, as it exceeds the doping density in the dark giving a $R_{\text{sh,e}^-}$ of $202\,\Omega$/sq. These results suggest that not only hole but electrons as well participate to the current flow in the bulk for illuminations higher than 7%.

TABLE IV: R_{sh} values of the TLM sample featuring the a-Si:H(p) layers with the high TMB flow for the different illuminations as well as the injection levels Δp and Δn assuming the R_{sh} being the one of holes ($R_{\text{sh,h}^+}$) or the one of electrons ($R_{\text{sh,e}^-}$), respectively.

Illumination (%)	R_{sh} (Ω/sq)	Δp (cm^{-3})	Δn (cm^{-3})
7	263	3.16×10^{15}	-
13	173	4.88×10^{15}	2.69×10^{14}
50	75	1.16×10^{16}	2.51×10^{15}
100	49	1.84×10^{16}	4.81×10^{15}

To complete these observations, Figure 7 plots the *I-V* curves of the different TLM gaps for the p-type CSPC with the a-Si:H(p) layer featuring a medium TMB flow deposited on a c-Si(n) wafer and for the different illumination of 7% (a), 13% (b), 50% (c) and 100% (d). Interestingly, at 7% illumination all the *I-V* curves are close to be superimposed, but the more the illumination increases, the more the curves separate and present the expected TLM trend as a function of the gap. This superposition of the *I-V* curves can be explained by a very high value of ρ_c (see Figure 5) whose contribution to the total resistance dominates significantly the R_{sh} one for low illumination. This increase of ρ_c for low illumination can also be observed in Figure 6a.

The combination of these two experimental evidences (the values of R_{sh} close to $R_{\text{sh,e}^-}$ ones and the superposition of the *I-V* curve at low illumination) reveal that the transport of the TLM current is supported thanks to transport mechanisms involving both carrier types (electrons and holes) and is dependent on the injection level. To deepen the understanding of these interesting physical phenomena, we performed additional investigations which are detailed in section III-C below.

TABLE V: Injected carrier densities obtained in the study [4] (for a n/N TLM sample with similar geometry and passivation quality than the p/N samples presented in this study) and which are expected for the present case study (expected Δn) for the four different illuminations along with the corresponding hole and electron R_{sh} ($R_{\text{sh,h}^+}$ and $R_{\text{sh,e}^-}$, respectively).

Illum. (%)	Expected Δn (cm^{-3})	$R_{\text{sh,h}^+}$ (Ω/sq)	$R_{\text{sh,e}^-}$ (Ω/sq)
7	2.85×10^{14}	2761	166
13	4.32×10^{14}	1827	153
50	1.91×10^{15}	422	86
100	5.20×10^{15}	160	45

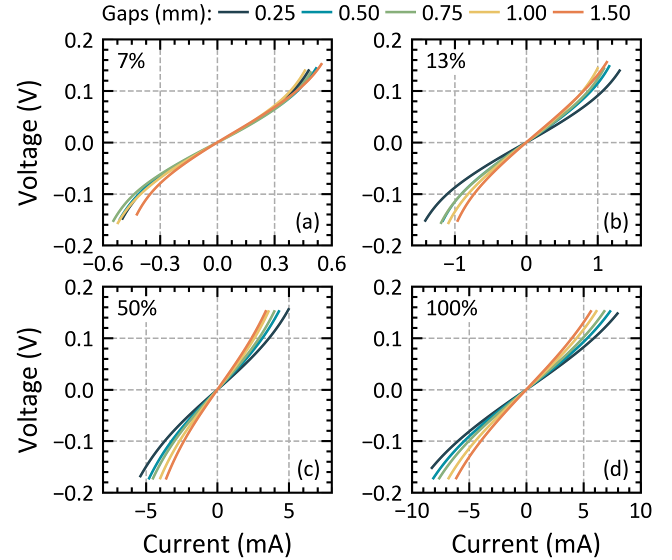

Fig. 7: *I-V* curves of the different TLM gaps of the p-type CSPC featuring the a-Si:H(p) layers with the medium TMB flow deposited on c-Si(n) wafer, for the case of (a) 7%, (b) 13%, (c) 50% and (d) 100% illumination.

C. Lateral transport in p/N TLM samples under illumination

As a first qualitative element of discussion about the role of illumination on the gap and each contact separately, Figure 8 presents the *I-V* curves of a TLM sample with a large gap of 4 cm under various conditions of masking (for various combination with the gap and TLM pads either masked or at 100% illuminated). First, under uniform illumination, it is observed that a current can flow in those p/N structure with a linear regime close to 0 V (green curve), as obtained previously in section III-B. Second, when the gap between the two pads is masked (orange curve), current can still flow laterally through the c-Si(n) wafer even in the absence of photo-generated carriers hereby. Then, masking the area under the two pads while keeping the gap illuminated, it is observed that no current flows (black curve, underneath the other dashed curves). The latter is due to the fact that in the dark the two p-n junctions present below both TLM pads are facing each other along the current path and thus block the current flow. This simple experiment reveals again that the photogenerated carriers make it possible to open the p-n junctions (see Figure

3). Finally, when at least one of the contact is illuminated, a current can flow either in forward or reverse bias (red and blue curves respectively). This can be explained again by the blocking p-n junction present below both pads, making the current pass only in one direction, while below the illuminated pad the wafer is conductive to holes and there is no p-n junction there. Moreover, those two cases combined together are superposed with the masked gap case (orange curve), which stems from a similar bulk resistivity since the total resistance is dominated by the c-Si(n) sheet resistance in those large TLM samples.

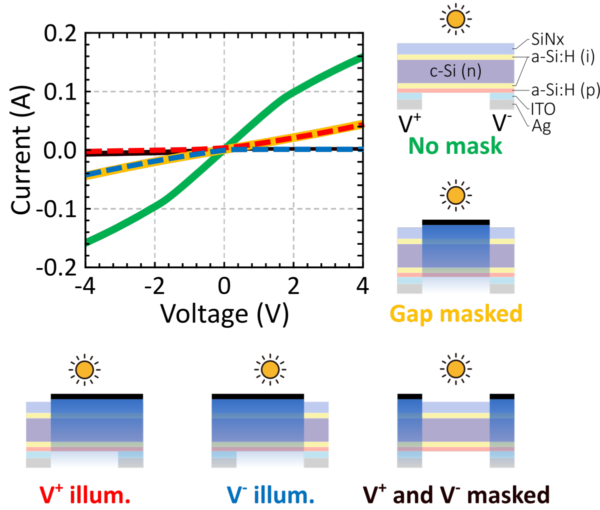

Fig. 8: *I*-*V* curves of the large TLM samples with a gap of 4 cm under uniform 100% illumination (No Mask), masking only the gap (Gap masked), illuminating only the positive (V^+ illum.) or negative (V^- illum.) pole, respectively, and finally with the two contact pads masked (V^+ and V^- masked). Note that for this last case, no current is flowing and the *I*-*V* curve is hidden behind the others (dark curve).

TABLE VI: R_{sh} values extracted from the large TLM samples under uniform 100 % illumination (No Mask) and with the gap masked (Gap Masked) as presented in Figure 8. In the dark, the base doping provides a R_{sh} of about 110 Ω/sq. For uniform illumination, the injection level Δn at a given illumination is extracted from PCD measurement directly on the finished sample. The numbers in parenthesis give the range of the variation on the obtained R_{sh} interpolated from the gap series.

	No Mask		Gap Masked
Illumination (Sun)	**Δn (cm^{-3})**	**R_{sh} (Ω/sq)**	**R_{sh} (Ω/sq)**
100%	1.17×10^{16}	22 (13-29)	110 (100-118)
45.4%	8.02×10^{15}	30 (19-40)	110 (99-120)
6.5%	2.42×10^{15}	54 (46-60)	114.6 (100-127)
1.7%	7.4×10^{14}	102 (82-120)	non-ohmic

Going one step further, Table VI gives the R_{sh} values obtained by measuring under illumination the 2 cm, 4 cm and 6 cm gap TLM samples. Once again, we find low values of R_{sh} as it was already presented in Table IV, indicating that the transport benefits from the high mobility of electrons. For

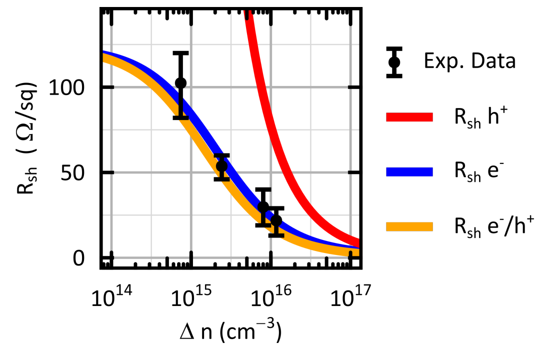

Fig. 9: R_{sh} as function of the injection level (Δn) measured on the large TLM samples and compared to the theoretical R_{sh} calculated considering only electrons conductivity ($R_{\text{sh,e}^-}$), only holes conductivity ($R_{\text{sh,h}^+}$), or the sum of both respectively ($R_{\text{sh,e}^-/\text{h}^+}$).

these peculiar large TLM samples, in the case of a uniform illumination, the injection corresponding to this illumination level at open circuit can be obtained from a direct PCD measurement on those samples thanks to the gaps which are larger than the measurement coil. From these measurements, it is observed in Figure 9 that the experimental curve of R_{sh} as a function of the injection level (Δn) matches with the theoretical values obtained considering either only electrons or electrons and holes combined in the transport through the c-Si(n) rather than considering a transport mediated by holes only. Finally, in Table VI when the gap is masked, the R_{sh} remains constant for all illuminations and corresponds within the error bounds to the R_{sh} of the electrons provided by the base doping of the c-Si(n) wafer, as measured from PCD measurement. In summary, despite the presence of two p-type CSPCs allowing only holes to flow through them, we demonstrated that the TLM current can flow laterally inside the c-Si(n) (i) thanks to the photo-generated carriers present at least below the TLM pads which open the p-n junction and (ii) that electrons are effectively participating to the TLM current rather than only holes as initially expected.

From there, taking into account the fact that the forward bias contact (TLM pad) needs to be illuminated for current to flow, our explanation for this phenomenon is that under illumination, the photogenerated carriers promote the transport inside the c-Si(n) thanks to recombination mechanisms. First, photogenerated-holes injected within a diffusion length of the positive TLM pad can be extracted and travel through the outside electric circuit. Then, these holes arrive at the edge of the negative TLM pad at a distance corresponding to a TLM transfer length (L_T). In parallel, the electrons (from photogeneration and/or doping) can travel through the c-Si(n) bulk with the electrons sheet resistance. Eventually, both charge carriers will have to recombine within the hole diffusion length (L_D) close to the negative TLM pad. This description of transport is given in Figure 10a.

In addition, as recombination mechanisms are supporting the transport here and are enhanced with the injected carrier density increases, this therefore promotes an important reduction of the ρ_c contribution with the illumination increase.

This could result, at low injection, in a very high value of ρ_c (dominating the value of $R_{\rm sh}$) because of a too low injected carrier density reached inside the c-Si(n) bulk which is not enough to support fully the recombination transport mechanisms. This may explain the superposition of the *I-V* curves at low illumination presented in Figure 7 and the presence of a transition state (between poor and efficient transport) from low to high illumination (see Figure 6).

To observe this transport mechanism supported by recombination experimentally, a PL setup was adapted in order to illuminate only one contact pad, similarly to how we proceeded for the previous *I-V* measurements presented on Figure 8 (red case), while being able to measure the radiative part of the recombination occurring under the second pad. Figure 10a presents the modified PL setup together with the physical mechanisms described in section III-B. Figure 10b presents the corresponding PL images taken with or without masking ("V+ illum" and "No Mask", respectively) and at different bias conditions (from 0 to 8 V). First, it is observed on the PL image without masking and at 0 V that it is possible to distinguish optically the contact pads since the silver pad absorb a part of the radiative emission. This makes it possible to align correctly our PL laser to illuminate only the positive pad. Then increasing the voltage, a lower PL signal at the left TLM pad is observed for both cases (No Mask and V^+ Illum), starting from the contact edge, while the signal increases on the right pad. This reveals that recombination mechanisms occur under the second pad, even if it was not illuminated. The absence of recombination in the c-Si(n) bulk when using a mask shows that no minority carrier (i.e. hole) diffuses there, which leaves the electrons as the only carrier type responsible for the transport in this region. They eventually recombine with holes traveling through the external circuit starting within a diffusion length of the right contact, as described in section III-C. Note that in the case where the pad distance starts to become small as compared to the diffusion length, holes can in principle diffuse from one contact to the other without recombining and support a larger share of the transport, thus increasing the measured R_{sh}. This could explain the higher sheet resistances obtained at lower illumination in Table IV since the design of those previous TLM samples features pad distances smaller than typical diffusion lengths. The accurate relationship between the measured $R_{\rm sh}$ and the injection level is expected to be related to the way each charge carriers participate to the transport, thus depending on the illumination level and the sample geometry. This has been already considered in [29] and should be investigated in further study. On the other hand, the relationship between ρ_c and Δn should remained unchanged as the energy-band diagram in the vicinity of the contact is not impacted by the transport of the holes at low bias applied by the TLM measurement.

Overall, these results demonstrated that the low $R_{\rm sh}$ under illumination obtained in TLM samples featuring p-type CSPCs deposited on n-type c-Si wafer corresponds to either a transport mediated by the electrons or the electrons and holes together rather than by the holes only as initially expected. This moreover implies that this electron transport in the bulk in the presence of two p-type CSPCs deposited on c-Si(n) can only be mediated thanks to photogeneration under one pad and recombination under the other (figure 10).

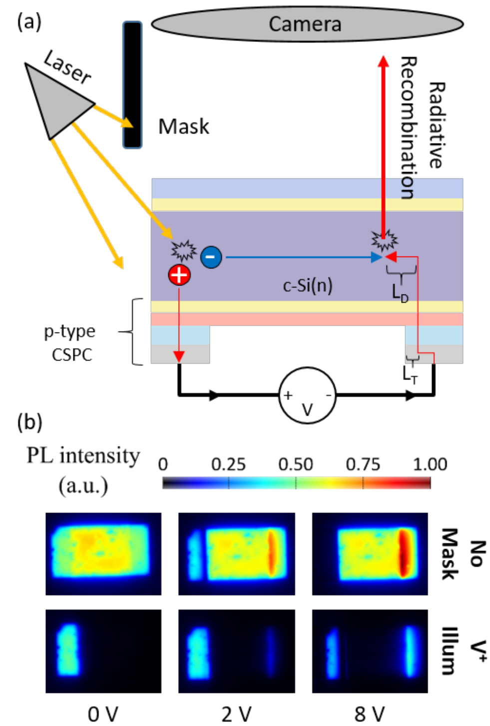

Fig. 10: (a) PL setup used to evidence the physical mechanisms allowing electrons to flow in between the two p-type CSPCs in p/N TLM samples under illumination, thanks to the (i) e^-/h^+ photo-generation, (ii) holes extraction through the external circuit, and (iii) the e^-/h^+ recombination. (b) Corresponding PL images taken at 1 sun and three different external voltages without mask and with only the left pad illuminated. The pads can be distinguished optically since they are not optimized for infrared reflection ($115\,\mathrm{nm}$ TCO / Ag).

IV. Conclusion

In this work, we demonstrated that the ρ_c of p-type CSPCs deposited on c-Si(p) wafer increase with the rise of the illumination, i.e., with the decrease of the illumination-impacted $R_{\rm sh}$. This behaviour was found to be similar to the case of n-type CSPCs deposited on c-Si(n) wafer presented in literature and in both cases, the orders of magnitude of the variation of ρ_c were found to be similar. In addition, the different p-type CSPCs under study present different slopes revealing different illumination responses depending on the a-Si:H(p) layer dopings, as was observed for n-type CSPCs deposited on c-Si(n). Furthermore, we studied and discussed the applicability of TLM measurements to measure p-type CSPCs deposited on n-type c-Si wafers. First, performing TLM measurement of such samples in dark condition was demonstrated to allow one to characterize sheet resistance values with orders of magnitude corresponding to the inversion layer inside the c-Si(n) wafer. Second, contrary to what has been observed for the case of CSPCs with same type as the bulk, the ρ_c values

were found to decrease with the illumination-impacted R_{sh} decrease. Measuring ρ_c at illumination yielding injection level close to the MPP of a solar cell lead to higher values than for p-type CSPCs deposited on c-Si(p) wafer measured in the dark. In addition, at sufficiently high illumination (i.e. above 50% illumination here), the ρ_c values obtained for a given p-type CSPC on c-Si(n) and c-Si(p) wafers are of the same order of magnitude. These results strongly suggest that to perform accurate series resistance breakdown of a given solar cell, the ρ_c of its two contacts (i.e., n and p-type CSPC) have to be measured on similar wafer type than the considered solar cell and under MPP injection. Finally, we demonstrated that the lateral transport inside the c-Si(n) bulk is supported by the electrons and not only by the holes in these p/N TLM samples thanks to two experimental proofs, i.e. that the R_{sh} evolution as function of injection behaves as the one of electrons or electrons together with holes, and that electron transport in the c-Si(n) bulk can only be mediated thanks to photogeneration under one TLM pad and recombination under the other. Eventually, the method of this work was applied to SHJ CSPCs but can be generalised to any solar cell technology. Overall, these work provides additional understanding of the TLM measurement under illumination as well as strong insights for the investigation of carriers transport and electrical losses in solar cells.

ACKNOWLEDGMENT

The authors would like to thank C. Allebé and P. Wyss for the wafer cleaning and texturization, N. Badel for the silver screen-printing metallization, M. Simmonds for the energy-band simulations and his help for the TLM measurements, as well as J. Geissbühler, A. Descoeudres and C. Allebé for their fruitful discussions. The authors would also like to acknowledge funding provided by the SNSF SHAMAN under Grant Agreement No. 200021_192310.

MATHEMATICAL FORMULAS

A. Transfer length method computation

The transfer length method (TLM) is one of the most commonly used techniques to measure the specific contact resistivity (ρ_c) of an individual material layer or of a stack of several material layers [6]–[9]. The total contact resistance (R_T) measured between two TLM pads with an interpad distance d can be expressed as:

$$R_T = \frac{R_{\text{sh}}}{w} \cdot d + 2 \cdot \left(\frac{\rho_c}{w \cdot L_T}\right) \cdot \coth\left(\frac{L}{L_T}\right), \tag{1}$$

where R_{sh} is the sheet resistance of the TLM conductive layer, w and L are the width and the length of the TLM pads respectively and L_T the transfer-length [8].

To perform TLM computation, R_T is measured for various interpad distances and plotted against each other resulting in a linear relation. Three parameters are extracted from this linear plot. First, the slope allows one to extract the value of R_{sh} of the conductive layer knowing the contact width w, which is independently measured, with the relation: $slope = R_{\text{sh}}/w$. Secondly, the x-intercept (d_0, with $d_0 < 0$) at $R_T = 0$ gives the transfer length by solving the implicit equation $L_T = -d_0/(2 \cdot \coth(L/L_T))$. Thirdly, knowing L_T, the y-intercept (R_{T0}) at d = 0 gives the contact resistance with $R_c = R_{T0}/2 = \frac{\rho_c}{w \cdot L_T} \cdot \coth(L/L_T)$. Finally, the contact resistivity is calculated using the relation

$$\rho_c = \frac{R_c \cdot w \cdot L_T}{\coth(L/L_T))} \tag{2}$$

B. Sheet resistance computation

For the injection dependant sheet resistances in n-type wafer, the following formula are used:

$$R_{sh,h^+}(\Delta n) = \frac{t}{\sigma_{h^+}} = \frac{t}{q\mu_h(p_0 + \Delta n)}, \tag{3}$$

$$R_{sh,e^-}(\Delta n) = \frac{t}{\sigma_{e^-}} = \frac{t}{q\mu_e(N_D + \Delta n)}, \tag{4}$$

$$R_{sh,e^-/h^+}(\Delta n) = \frac{t}{\sigma_{h^+} + \sigma_{e^-}} \tag{5}$$

$$= \frac{t}{q\mu_h(p_0 + \Delta n) + q\mu_e(N_D + \Delta n)} \tag{6}$$

where t is the wafer thickness, σ_{h^+} and σ_{e^-} are the conductivity of holes and electrons respectively, μ_h and μ_e their injection dependant mobilities which can be calculated using Klaasen's formula [16], p_0 the equilibrium holes concentration and N_D the donor concentration.

REFERENCES

[1] K. Yoshikawa, H. Kawasaki, W. Yoshida, T. Irie, K. Konishi, K. Nakano, T. Uto, D. Adachi, M. Kanematsu, H. Uzu, and K. Yamamoto, "Silicon heterojunction solar cell with interdigitated back contacts for a photoconversion efficiency over 26%," *Nature Energy*, vol. 2, no. 5, 2017.

[2] R. V. K. Chavali, S. De Wolf, and M. A. Alam, "Device physics underlying silicon heterojunction and passivating-contact solar cells: A topical review," *Progress in Photovoltaics: Research and Applications*, vol. 26, no. 4, pp. 241–260, apr 2018. [Online]. Available: http://doi.wiley.com/10.1002/pip.2959

[3] P. Procel, H. Xu, L. Mazzarella, L.-L. Senaud, B. Paviet-Salomon, H. Radhakrishna, M. Filipic, M. Xu, M. Boccard, A. Fioretti, R. Monnard, J. Stang, P. Wagner, D. Meza, D. Lachenal, B. Strahm, W. Duan, A. Lambertz, A. Fejfar, K. Ding, M. Despeisse, I. Gordon, L. Korte, C. Ballif, O. Isabella, and M. Zeman, "On the Correlation between Contact Resistivity and High Efficiency in (IBC-) SHJ Solar Cells," in *Proceedings of the 36th European Photovoltaic Solar Energy Conference and Exhibition (2019) 2CO.12.6*, 2019, pp. 251–254.

[4] L.-L. Senaud, P. Procel, G. Christmann, A. Descoeudres, J. Geissbühler, C. Allebé, N. Badel, P. Wyss, M. Boccard, O. Isabella, M. Zeman, S. Nicolay, M. Despeisse, C. Ballif, and B. Paviet-Salomon, "Advanced method for electrical characterization of carrier-selective passivating contacts using transfer-length-method measurements under variable illumination," *Journal of Applied Physics*, vol. 129, no. 19, p. 195707, may 2021. [Online]. Available: https://aip.scitation.org/doi/10.1063/5.0042854

[5] P. Procel, H. Xu, A. Saez, C. Ruiz-Tobon, L. Mazzarella, Y. Zhao, C. Han, G. Yang, M. Zeman, and O. Isabella, "The role of heterointerfaces and subgap energy states on transport mechanisms in silicon heterojunction solar cells," *Progress in Photovoltaics: Research and Applications*, no. March, pp. 1–11, 2020. [Online]. Available: https://doi.org/10.1002/pip.3300

[6] H. H. Berger, "Contact Resistance and Contact Resistivity," *Journal of The Electrochemical Society*, vol. 119, no. 4, p. 507, 1972.

[7] R. Halevy, "A Method for measuring the specific interface resistivity between two semiconductor layers and its application to a heavily doped n-type InP / GaInAs heterostructure Ran Halevy," Ph.D. dissertation, Technion - Israel Institute of Technology Sivan, 2011.

[8] H. H. Berger, "Models for contacts to planar devices," *Solid State Electronics*, vol. 15, no. 2, p. 145, 1972.

[9] D. K. Schroder and D. L. Meier, “Solar Cell Contact Resistance—A Review,” *IEEE Transactions on Electron Devices*, vol. 31, no. 5, pp. 637–647, 1984.

[10] D. Lachenal, D. Baetzner, W. Frammelsberger, B. Legradic, J. Meixenberger, P. Papet, B. Strahm, and G. Wahli, “Heterojunction and Passivated Contacts: A Simple Method to Extract Both n/tco and p/tco Contacts Resistivity,” *Energy Procedia*, vol. 92, pp. 932–938, 2016.

[11] C. Luderer, C. Messmer, M. Hermle, and M. Bivour, “Transport Losses at the TCO/a-Si:H/c-Si Heterojunction: Influence of Different Layers and Annealing,” *IEEE Journal of Photovoltaics*, vol. 10, no. 4, pp. 952–958, 2020.

[12] L. Basset, W. Favre, O. Bonino, J. Sudre, M. Gilles, and J.-P. Vilcot, “In depth analysis of transfer length method application on passivated contacts under illumination,” *Solar Energy Materials and Solar Cells*, vol. 230, no. July, 2021.

[13] L. Antognini, L.-L. Senaud, D. Türkay, L. Marthey, J. Dréon, B. Paviet-Salomon, M. Despeisse, M. Boccard, and C. Ballif, “Contact resistivity measurements and their applicability for accurate series resistance breakdown in heterojunction solar cell,” *AIP Conference Proceedings*, vol. 2487, no. 1, p. 020002, 2022. [Online]. Available: https://aip.scitation.org/doi/abs/10.1063/5.0090643

[14] A. Shah, C. Ballif, W. Beyer, F. Finger, and H. Schade, *Thin-Film Silicon Solar Cells*. EPFL press, 2010.

[15] S. Eidelloth and R. Brendel, “Analytical theory for extracting specific contact resistances of thick samples from the transmission line method,” *IEEE Electron Device Letters*, vol. 35, no. 1, pp. 9–11, 2014.

[16] D. B. M. Klaassen, “A Unified Mobility Model for Device Simulation - I. Model Equation and Concentration Dependence,” *Solid State Electronics*, vol. 35, no. 7, pp. 953–959, 1992.

[17] D. B. Klaassen, “A unified mobility model for device simulation-II. Temperature dependence of carrier mobility and lifetime,” *Solid State Electronics*, vol. 35, no. 7, pp. 961–967, 1992.

[18] A. Descoeudres, L. Barraud, S. De Wolf, B. Strahm, D. Lachenal, C. Guérin, Z. C. Holman, F. Zicarelli, B. Demaurex, J. Seif, J. Holovsky, and C. Ballif, “Improved amorphous/crystalline silicon interface passivation by hydrogen plasma treatment,” *Applied Physics Letters*, vol. 99, no. 12, pp. 2009–2012, 2011.

[19] A. Descoeudres, J. Geissbiihler, J. Horzel, A. Lachowicz, J. Levrat, S. M. de Nicolas, S. Nicolay, B. Paviet-Salomon, L.-L. Senaud, A. Tomasi, C. Ballif, C. Allebe, M. Despeisse, N. Badel, L. Barraud, J. Champliaud, G. Christmann, L. Curvat, F. Debrot, and A. Faes, “Advanced silicon thin films for high-efficiency silicon heterojunction-based solar cells,” *2017 IEEE 44th Photovoltaic Specialist Conference (PVSC), Washington, DC*, pp. 50–55, 2017.

[20] L.-L. Senaud, G. Christmann, A. Descoeudres, J. Geissbuhler, L. Barraud, N. Badel, C. Allebe, S. Nicolay, M. Despeisse, B. Paviet-Salomon, and C. Ballif, “Aluminium-Doped Zinc Oxide Rear Reflectors for High-Efficiency Silicon Heterojunction Solar Cells,” *IEEE Journal of Photovoltaics*, vol. 9, no. 5, pp. 1217–1224, 2019.

[21] R. A. Sinton, A. Cuevas, and M. Stuckings, “Quasi-stead-state photoconductance, a new method for solar cell material and device characterization,” *Conference Record of the Twenty Fifth IEEE Photovoltaic Specialists Conference*, pp. 457–460, 1996.

[22] T. Trupke, R. A. Bardos, M. C. Schubert, and W. Warta, “Photoluminescence imaging of silicon wafers,” *Applied Physics Letters*, vol. 89, no. 4, pp. 1–4, 2006.

[23] L.-L. Senaud, “Electrical Losses Mitigation in Silicon Heterojunction Solar Cells,” Ph.D. dissertation, EPFL, 2021.

[24] M. Filipič, Z. C. Holman, F. Smole, S. De Wolf, C. Ballif, and M. Topič, “Analysis of lateral transport through the inversion layer in amorphous silicon/crystalline silicon heterojunction solar cells,” *Journal of Applied Physics*, vol. 114, no. 7, 2013.

[25] O. Maslova, A. Brézard-Oudot, M. E. Gueunier-Farret, J. Alvarez, W. Favre, D. Muñoz, and J. P. Kleider, “Understanding inversion layers and band discontinuities in hydrogenated amorphous silicon/crystalline silicon heterojunctions from the temperature dependence of the capacitance,” *Applied Physics Letters*, vol. 103, no. 18, 2013.

[26] D. A. Clugston and P. A. Basore, “PC1D version 5: 32-bit solar cell modeling on personal computers,” *Conference Record of the IEEE Photovoltaic Specialists Conference*, pp. 207–210, 1997.

[27] D. K. Schroder, *Semiconductor Material and Device Characterization*, third edit ed. John Wiley & Sons, 2006.

[28] T. Kamioka, Y. Hayashi, K. Gotoh, T. Hara, R. Ozaki, M. Morimura, A. Shimizu, K. Nakamura, N. Usami, A. Ogura, and Y. Ohshita, “Simulation study on lateral minority carrier transport in the surface inversion layer of the p-aSi : H / i-aSi : H / cSi heterojunction solar cell,” *Japanese Journal of Applied Physics*, vol. 60, no. 2, p. 026503, 2021.

[29] L. M. Antognini, “Contact design for silicon heterojunction solar cells,” p. 215, 2022. [Online]. Available: http://infoscience.epfl.ch/record/294790